^{1}H NMR Studies of Aliphatic Ligand Binding to Human Plasminogen Kringle 4†

Andrew M. Petros,‡ Vasudevan Ramesh,§ and Miguel Llinás*
Department of Chemistry, Carnegie Mellon University, Pittsburgh, Pennsylvania 15213
Received July 29, 1988

ABSTRACT: A detailed ^{1}H NMR analysis of ligand binding to the human plasminogen kringle 4 domain has been carried out at 300 MHz. The ligands that were investigated are N^{α}-acetyl-L-lysine, L-lysine methyl ester, N^{α}-acetyl-L-lysine methyl ester, L-lysine hydroxamic acid, *trans*-(aminomethyl)cyclohexanecarboxylic acid (AMCHA), and 4-(aminomethyl)bicyclo[2.2.2]octane-1-carboxylic acid (AMBOC). Specific ligand-binding effects were detected via two-dimensional COSY experiments. The side chains that are the most perturbed by ligand presence are those from Trp^{62}, Phe^{64}, and Trp^{72}. Ligand–kringle saturation transfer (Overhauser) experiments show that the aromatic rings from these three residues, especially Trp^{72}, are in direct contact with the ligand. These results add support to a previously reported model of the kringle 4 lysine-binding site [Ramesh, V., Petros, A. M., Llinás, M., Tulinsky, A., & Park, C. H. (1987) *J. Mol. Biol. 198*, 481–498] by which these aromatic groups are assigned a key role in establishing hydrophobic interactions with the ligand molecule. Equilibrium association constants (K_a) and kinetic rate constants (k_{on}, k_{off}) were determined for the binding of the various linear and cyclic ligands to kringle 4. We find that those ligands whose carboxylate function is blocked bind significantly weaker ($K_a \lesssim 2$ mM^{-1}) than the corresponding analogues where the anionic center is present ($K_a \gtrsim 20$ mM^{-1}), which underscores the relevance of the polar group in stabilizing the interaction with the kringle 4 binding site. Furthermore, AMBOC ($K_a \sim 48$ mM^{-1}) exhibits weaker binding than AMCHA ($K_a \sim 159$ mM^{-1}), a fact that reflects the relative values of the dissociation rate constants ($k_{off} \sim 3.8$ and 1.3 s^{-1}, respectively) and that suggests a more constrained fit of the bulkier ligand at the binding site. Of all the investigated ligands, AMCHA is the one that exhibits the highest affinity for kringle 4. The numerical data are discussed in terms of optimal ligand structure and requirements for fibrin binding in vivo.

Plasmin and its inactive precursor, plasminogen, play central roles in fibrinolysis and in overall hemostasis (Collen, 1980; Wallén, 1980). The native enzyme consists of two chains, a heavy chain of $M_r \sim 57\,000$ and a light chain of $M_r \sim 25\,000$, held together by two disulfide bonds. The heavy chain is composed of five kringle modules, of $M_r \lesssim 10{,}000$ each, while the light chain forms the catalytic site (Claeys et al., 1976; Sottrup-Jensen et al., 1978). The kringles are independent structural, folding, and functional domains (Sottrup-Jensen et al., 1978; Trexler & Patthy, 1983; Castellino et al., 1981; Novokhatny et al., 1984), and it has been postulated that they are responsible for the attachment of plasmin and plasminogen to the fibrin clot (Wiman & Collen, 1978). Furthermore, the kringle 1 and kringle 4 domains have been shown to bind L-lysine and a number of lysine analogues (Sottrup-Jensen et al., 1978; Lerch et al., 1980; Winn et al., 1980). This lysine-binding ability is thought to be intimately related to the high affinity of plasminogen and plasmin for fibrin (Wiman & Collen, 1978; Lucas et al., 1983; Christensen, 1984; Bok & Mangel, 1985).

In light of the above, much of the research effort in our laboratory has been aimed at characterizing ligand binding to the kringle 4 fragment from plasminogen. Given its size and the fact that it can be readily isolated in good yields via elastase digestion of the zymogen (Sottrup-Jensen et al., 1978), kringle 4 affords a most suitable globular polypeptide for NMR experimentation. The initial NMR studies of ligand binding to K4[1] focused mainly on qualitative analysis of ligand effects via 1D spectroscopy and development of a framework for the determination of the equilibrium binding (K_a) and kinetic association/dissociation (k_{on}/k_{off}) constants (Hochschwender et al., 1983; Llinás et al., 1985; De Marco et al., 1986, 1987). Recently, we have begun to analyze lysine binding to kringle 4 by exploiting 2D NMR techniques, which has led to a better understanding of the ligand–kringle interaction (Ramesh et al., 1987). Furthermore, the ligand-binding data, combined with proton Overhauser studies, have enabled us to generate a model of the kringle 4 lysine-binding site from the recently solved X-ray crystallographic structure

Chart I: Linear Aliphatic Ligands

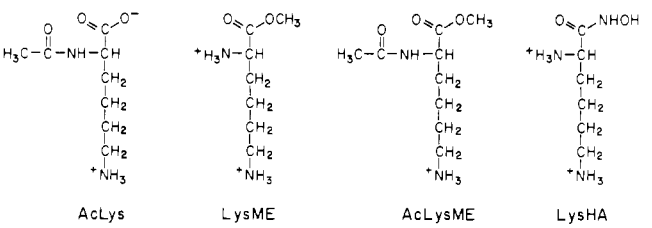

† This research was supported by the U.S. Public Health Service, NIH Grant HL 29409.
‡ Present address: Smith Kline & French Laboratories, P.O. Box 1539, L-940, King of Prussia, PA 19406-0939.
§ Present address: Department of Biochemistry, University of Leicester, Leicester LE17RH, England.

[1] Abbreviations: AcLys, N^{α}-acetyl-L-lysine; AcLysME, N^{α}-acetyl-L-lysine methyl ester; AMBOC, 4-(aminomethyl)bicyclo[2.2.2]octane-1-carboxylic acid; AMCHA, *trans*-(aminomethyl)cyclohexanecarboxylic acid; COSY, two-dimensional chemical-shift-correlated spectroscopy; ϵACA, ϵ-aminocaproic acid (6-aminohexanoic acid); FID, free induction decay; K, kringle; K_a, ligand–kringle equilibrium association constant; k_{off}, ligand–kringle dissociation rate constant; k_{on}, ligand–kringle association rate constant; LysHA, L-lysine hydroxamic acid; LysME, L-lysine methyl ester; NOE, nuclear Overhauser effect; pH*, glass electrode pH reading uncorrected for deuterium isotope effect; rf, radio frequency; 1D, one-dimensional; 2D, two-dimensional.

0006-2960/89/0428-1368$01.50/0

Chart II: Cyclic Aliphatic Ligands

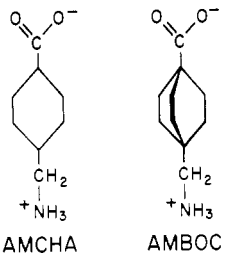

of prothrombin fragment 1 (Ramesh et al., 1987; Park & Tulinsky, 1986).

The work reported here focuses on an analysis of the binding of several new ligands to the human plasminogen kringle 4. It has been shown previously by several groups that the ligands which interact most strongly with plasminogen and with plasminogen fragments, such as kringle 4 and kringle 1 + 2 + 3, are all zwitterionic, with a dipole distance of ~6.8 Å (Okamoto et al., 1968; Markwardt, 1978; Winn et al., 1980). Furthermore, many of these ligands have been shown to exhibit potent antifibrinolytic activity (Markwardt, 1978). Since the purported physiological ligand of kringle 4 is lysine, most likely lysyl side chains exposed on the fibrin surface, four of the ligands we have chosen to study are direct derivatives of L-lysine. They are N^{α}-acetyl-L-lysine (AcLys), L-lysine methyl ester (LysME), N^{α}-acetyl-L-lysine methyl ester (AcLysME), and L-lysine hydroxamic acid (LysHA) (Chart I). These ligands have allowed us to examine the effect on lysine binding of blocking the α-amino group (AcLys), the carboxyl group (LysME, LysHA), and both the α-amino and carboxyl groups (AcLysME). The other two ligands we have investigated (Chart II) are cyclic, *trans*-(aminomethyl)cyclohexanecarboxylic acid (AMCHA), and bicyclic, 4-(aminomethyl)-bicyclo[2.2.2]octane-1-carboxylic acid (AMBOC), lysine analogues. Although they lack an α-amino group, they are both zwitterionic, and since they exhibit the "optimal" dipole distance of ~6.8 Å, they can be considered to be sterically rigid analogues of lysine. Furthermore, they possess bulky cyclohexyl and bicyclohexyl moieties and, hence, are expected to perturb the kringle 4 NMR spectrum to a greater extent than the linear ligands. This has helped us to determine which amino acid side chains interact with the ligand at the binding site, and from ligand–kringle magnetization transfer (Overhauser) experiments, we have been able to identify points of protein–ligand contact. Finally, the magnitudes of the kringle–ligand association/dissociation constants (K_a, k_{on}, k_{off}) have provided further insights into the relevance of hydrophobic surfaces for ligand binding while affording unambiguous evidence that peptides containing carboxy-terminal lysyl residues are the most likely candidates to act as kringle ligands in vivo.

Materials and Methods

Plasminogen was purified from whole, outdated human blood plasma (a gift of the Central Blood Bank of Pittsburgh) essentially by the method of Deutsch and Mertz (1970); the two affinity forms were then separated by the method of Brockway and Castellino (1972). Kringle 4 was generated via elastase digestion of plasminogen according to previously published methods (Sottrup-Jensen et al., 1978; Winn et al., 1980). Prior to performing the NMR experiments, labile amide protons were exchanged for deuterons by incubating the K4 samples in ^2H_2O, pH* 7, at 310 K for 3 h. The samples were then lyophilized exhaustively. Each sample was then dissolved in ^2H_2O and further lyophilized twice in order to remove residual $^1H^2HO$. Finally, the kringle 4 samples were dissolved in 0.35–0.4 mL of ^2H_2O and placed into 5-mm NMR tubes. The pH* of the samples was adjusted with dilute ^2HCl or NaO^2H.

AcLys, LysME, AcLysME, and LysHA were obtained from Sigma Chemical Co.; ϵACA and AMCHA originated from Aldrich Chemical Co. AMBOC was a gift of Dr. R. Hirschmann, Merk, Sharp and Dohme Research Laboratories, Rahway, NJ. Solvent ^2H_2O was purchased from Merk, Sharp and Dohme, Ltd., Montreal, Canada.

^1H NMR spectra were recorded in the Fourier mode at 300 MHz on a Bruker WM-300 NMR spectrometer under Aspect 2000 minicomputer control, interfaced to either Diablo 44 or Winchester disk drives. 1D spectra were acquired with quadrature detection, and resolution enhancement, whenever implemented, was achieved by Gaussian multiplication (Ferrige & Lindon, 1978). Chemical shifts are referred to the sodium (trimethylsilyl)[2,2,3,3-^2H]propionate resonance frequency using *p*-dioxane as an internal standard (De Marco, 1977), and shifts to low fields are defined as positive. The temperature inside the spectrometer probe was measured with a calibrated methanol sample.

Truncated driven NOE experiments (Dubs et al., 1979) were carried out by pseudoselectively irradiating a transition for fixed time, usually 0.1–0.5 s, followed immediately by data acquisition. In order to minimize the effects of long-term instrumental instabilities, the frequency setting of the presaturation pulse was first placed on-resonance, and 16 scans were collected and subtracted in-memory from an equal number of off-resonance experiments. Typically, 500–1000 such cycles of 16 scans each were acquired in order to achieve a satisfactory signal-to-noise ratio.

COSY spectra (Nagayama et al., 1980; Wider et al., 1984) were acquired with 512 equally spaced evolution time period, t_1, values, and each t_1 spectrum was averaged over 288 transients. The spectral width in the t_2 direction was usually about 3200 Hz with a block size of 2K data points. Quadrature detection was employed in both directions, and phase cycling procedures that select for N-type peaks were implemented. The residual $^1H^2HO$ resonance was suppressed by gated, low-power irradiation during the relaxation delay of 2.3 s which was introduced between scans. Prior to Fourier transformation the time domain data matrix was zero-filled to 1K in the t_1 direction and multiplied by a sine bell weighting function. Thus, a frequency domain data matrix of 1K × 1K was obtained that gave a digital resolution of ~3.2 Hz along both δ_1 and δ_2. All COSY spectra are shown in the absolute value mode as symmetrized contour plots.

Results and Discussion

Ligand-Binding Effects. Human plasminogen kringle 4 has one Phe residue at position 64, three Trp residues at positions 25, 62, and 72, three His residues at positions 3, 31, and 33, and five Tyr residues at positions 2, 9, 41, 50, and 74. Most of the aromatic resonances are perturbed upon ligand binding, the exception being Tyr^2, His^3, Tyr^9, and Tyr^{50} (De Marco et al., 1986; Ramesh et al., 1987). In contrast, few of the aliphatic resonances are affected to any measurable extent (Petros et al., 1988a). Figure 1A shows, expanded, part of the aromatic COSY spectrum of ligand-free K4. Cross-peaks from four of the five tyrosines are visible in this region along with those denoting Phe^{64}, Trp^{62}, and Trp^{72} connectivities.[2]

[2] The Trp^{25} and Trp^{62} indole spin systems have not, as yet, been assigned to the individual amino acids residues. There is, however, good structural evidence which suggests that the assignments assumed here are correct (Llinás et al., 1985; Motta et al., 1987).

Table I: Ligand-Induced Shifts on Kringle 4 Aromatic Ring Proton Resonances

residue	multiplet[a]	proton	shift ($\Delta\delta \times 10^3$ ppm)[b] AcLys	LysME	AcLysME	AMCHA	AMBOC
Trp^{25}	s	H2	+25	+20	+25	+41	+16
	d	H4	+32	+32	+44	+56	+84
	t	H5	+45	+52	+45	+129	+74
	t	H6	+22	+25	+22	+82	+58
	d	H7				+23	+12
Trp^{62}	s	H2	+25	+15	+25	+37	+43
	d	H4	+75	+49	+75	+66	+79
	t	H5	+146	+122	+172	+310	+288
	t	H6	+39	+23	+39	+67	+142
	d	H7	−253	−253	−227	−290	−177
Trp^{72}	s	H2		−16		−18	+22
	d	H4		+12	+36		
	t	H5	−63	−64	−44	−16	
	t	H6	−14		+10		+10
	d	H7	+88	+106	+113	+86	+86
Tyr^{41}	d	H2,6	+10	+10	+38	+10	+19
	d	H3,5	+14	+16	+40	+18	+23
Tyr^{74}	d	H2,6	−21	−18		−26	−63
	d	H3,5	−53	−104	−53	−46	−77
Phe^{64}	t	H3,5		+18	+36	+14	−33
	t	H4	+145	+141	+194	−32	+17
His^{31}	s	H2	+6	+19	+6	+13	+27
	s	H4	+12	+40	+30	0	+31
His^{33}	s	H2	0	+24	+21	−60	−34
	s	H4	0	+27	+26	−52	−41

[a] Abbreviations: s, singlet; d, doublet; t, triplet. [b] Shifts are for kringle 4 in the presence of excess ligand and are referred to the respective ring proton frequencies in the absence of ligand. $\Delta\delta > 0$ (<0) signifies a ligand-induced low- (high-) field shift. For doublets and triplets, shifts $|\Delta\delta| < 0.01$ ppm are not listed.

The effect of ligand binding on these resonances is illustrated in the five remaining panels (Figure 1B–F) which show, each, the COSY spectrum of K4 recorded in the presence of an excess of ligand (heavy trace) superimposed on that of the ligand-free K4 (light trace). Values for the ligand-induced shifts are listed in Table I.

From inspection of Figure 1, it is apparent that there are some similarities as well as some differences in the way the various ligands perturb the aromatic resonances. The Trp^{72} H7 doublet is perturbed in an essentially uniform fashion by all five of the ligands which shift it by ~0.10 ppm to low fields.[3] The Trp^{62} H7 resonance is perturbed in the same way by AcLys, LysME, AcLysME, and AMCHA ($\Delta\delta \sim -0.25$ ppm), but it is somewhat less affected by AMBOC ($\Delta\delta \sim -0.18$ ppm). In contrast, the Phe^{64} H4 triplet is perturbed variously by the five ligands: it undergoes a large shift to low field with AcLys ($\Delta\delta = 0.145$ ppm), LysMe ($\Delta\delta = 0.141$ ppm), and AcLysME ($\Delta\delta = 0.194$ ppm) but is minimally affected by AMBOC ($\Delta\delta = 0.017$ ppm) and AMCHA ($\Delta\delta = -0.032$ ppm). Since, in contrast to what is the case with the three lysyl derivatives, AMCHA and AMBOC lack C^α substituents, it is apparent that the Phe^{64} side chain is sensitive to the ligand α-amino or N^α-acetyl group. This is consistent with our previous observation that the Phe^{64} side chain is affected by the stereoisomerism at the ligand C^α position (Ramesh et al., 1987).

Tyr^{41} also exhibits a measurable sensitivity to the various effectors (Figure 1C–F). However, it is the two more rigid and relatively bulkier ligands, AMCHA and AMBOC, that cause the most noticeable effects on the Tyr^{41} spectrum (Figure 1E,F). Hence, Tyr^{41} is probably close to the binding site although, as indicated by intermolecular (ligand–kringle) Overhauser experiments (vide infra), it is not likely to interact directly with the ligand (Ramesh et al., 1987). A similar trend

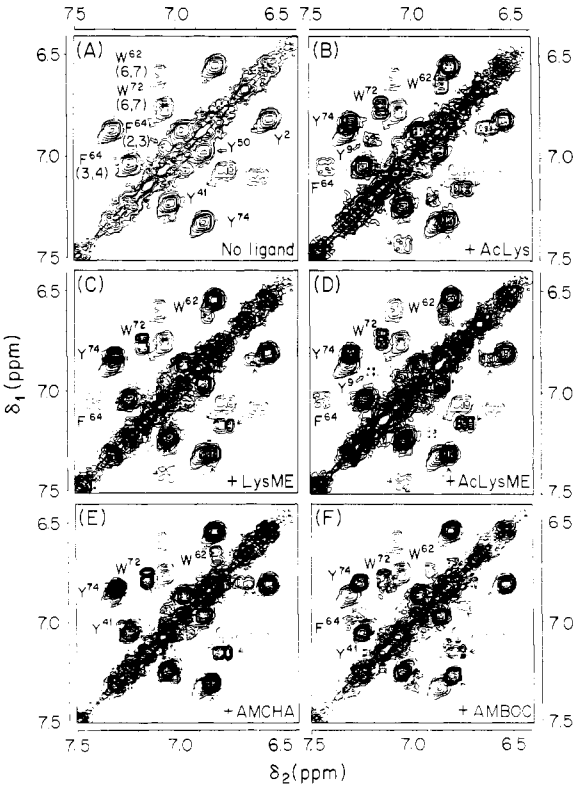

FIGURE 1: ^{1}H NMR COSY spectra of kringle 4: ligand effects on aromatic resonances. (A) Ligand-free kringle 4. Cross-peaks are labeled by two-digit numbers where the first digit labels the row proton and the second digit labels the column proton. (B–F) Spectra of kringle 4 saturated with ligand (heavy trace) are shown superimposed on the spectrum of ligand-free kringle 4 (light trace). Kringle concentration ~1 mM, pH* 7.2, 310 K; [ligand]/[kringle] ~3 for AcLys, AMCHA, and AMBOC and ~10 for LysME and AcLysME.

is that exhibited by the Tyr^{74} aromatic resonances, which are perturbed by all five of the tested ligands, with AMBOC causing the greatest overall effect. AMBOC binding shifts

[3] Shifts >0 (<0) denote a resonance move to a low- (high-) field position.

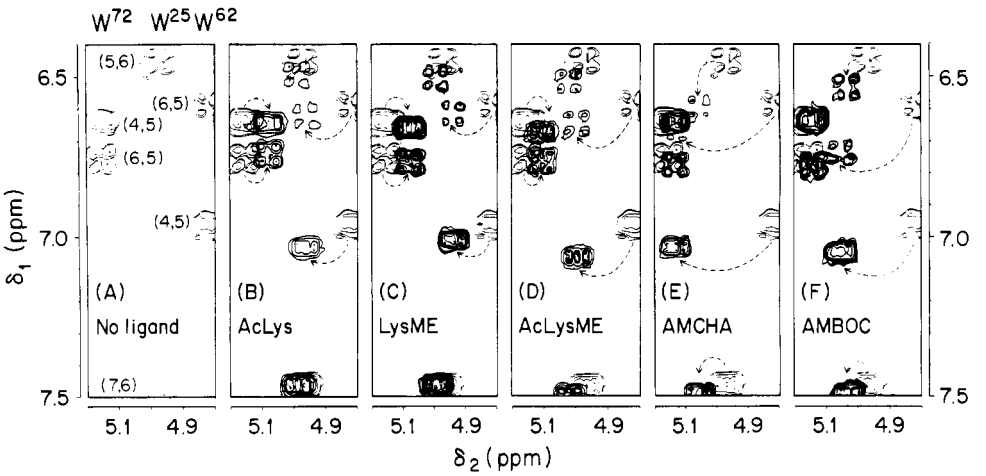

FIGURE 2: ^{1}H NMR COSY spectra of kringle 4: ligand effects on Trp indole resonances. (A) Ligand-free kringle 4. (B–F) Spectra of kringle 4 saturated with ligand (heavy trace) are shown superimposed on the spectrum of ligand-free kringle (light trace). Labeling of cross-peaks and experimental conditions are the same as for Figure 1.

the Tyr^{74} ortho (H2,6) and the meta (H3,5) doublets by $\Delta\delta$ = 0.063 and −0.077 ppm, respectively. Thus, the Tyr^{74} side chain is also likely to play some role in ligand binding although, as is the case with Tyr^{41}, it probably does not contact the ligand as closely as the Trp^{62}, Phe^{64}, and Trp^{72} aromatic rings do (Ramesh et al., 1987). In contrast, the Tyr^2 and Tyr^{50} cross-peaks show virtually no shift upon ligand binding (Figure 1).

The Tyr^9 ortho–meta connectivity shows up only in the presence of AcLys (Figure 1B) or AcLysME (Figure 1D). In the presence of the other ligands, and for ligand-free K4, the Tyr^9 resonances appear to be too broad to be detectable. It has already been shown in our laboratory (De Marco et al., 1985b; Ramesh et al., 1986; Petros et al., 1988b) that the appearance of Tyr^9 signals is highly dependent on temperature, observational frequency, and ligand presence. At 600 MHz, 293 K, with no added ligand, the Tyr^9 phenol ring protons exhibit an ABCD-type spectral pattern. When the temperature is raised to 310 K, the Tyr^9 resonances broaden beyond detection. Furthermore, at 300 MHz, 310 K, in the presence of ϵACA, the Tyr^9 resonances yield an AA′BB′ pattern. Thus, on going from 600 MHz, 293 K, to 300 MHz, 310 K, the ring flip dynamics of Tyr^9 changes from slow to fast on the NMR time scale. From Figure 1 it is clear that the observation of Tyr^9 signals at 300 MHz, 310 K, is dependent on the nature of the ligand. It is possible that this behavior of Tyr^9 is an indirect manifestation of the differing on–off exchange kinetics of the five ligands and/or the state of aggregation of the protein, an effect that we now know is blocked by ligand presence (Ramesh et al., 1986).

Figure 2 shows the effect of ligand binding on some of the Trp indole COSY cross-peaks that appear in the 4.8 ppm $\lesssim \delta_2 \lesssim$ 5.2 ppm region, well off the diagonal in the 2D spectrum, and hence not included in Figure 1. The Trp^{62} H5 resonance clearly experiences the largest shift upon ligand binding; it moves ~0.15 ppm with the three lysyl ligands and ~0.30 ppm with the cyclic ligands. The observation that this resonance is perturbed essentially the same way by the lysine derivatives and nearly twice as much by the cyclic analogues suggests that the Trp^{62} indole ring interacts with the central area of the ligand molecule, i.e., with the C$^\beta$ and C$^\gamma$ positions of AMCHA and AMBOC. Further evidence for this interpretation is provided by the behavior of the Trp^{62} H6 resonance which is perturbed nearly twice as much by AMCHA as by the lysyl ligands and nearly three times as much by AMBOC, the bulkiest of all the analogues (Figure 1, Table I).

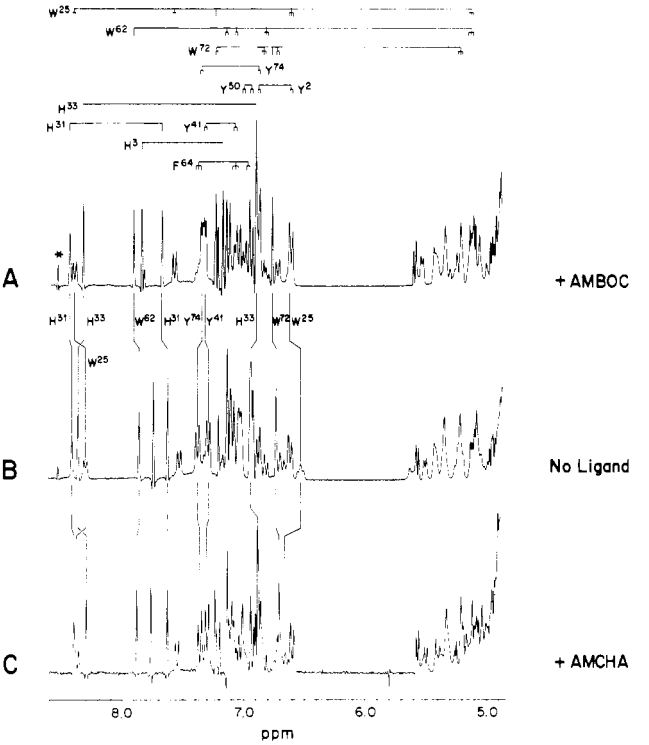

FIGURE 3: ^{1}H NMR spectra of kringle 4: effect of cyclic ligands on aromatic resonances. (A) Kringle 4 in the presence of AMBOC; (B) ligand-free kringle 4; (C) kringle 4 in the presence of AMCHA. Connectivities for the aromatic spin systems are indicated above spectrum A. Kinked vertical lines connect corresponding resonances in the three spectra. Experimental conditions are as for Figure 1. Spectra are shown resolution enhanced. An impurity signal is indicated (*).

It is interesting to note the different ways in which Trp^{25} and Trp^{72} respond to ligand presence (Figure 2, Table I). Overall, the Trp^{72} resonances are perturbed to a greater extent by the lysine derivatives than by the cyclic ligands, whereas the contrary is true for the Trp^{25} resonances. Thus, the Trp^{72} side chain, as is the case for Phe^{64}, is probably closer to the ligand C$^\alpha$ position at the binding site as it appears to sense the α-amino substituents of the lysyl ligands. The Trp^{25} indole ring, on the other hand, is likely to interact more—either directly or indirectly—with the central atoms of the ligand molecule since, as is the case for Trp^{62}, it senses the bulkiness of the effectors at the C$^\beta$ and C$^\gamma$ positions.

The effects of AMBOC and AMCHA on the Trp^{62}, Trp^{72},

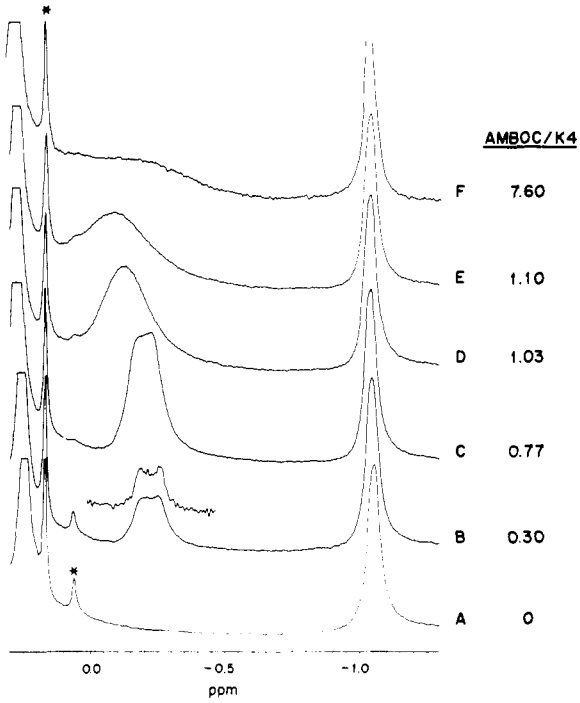

FIGURE 4: ^{1}H NMR high-field spectra of the kringle 4/AMBOC complex. The resonance at ~−1.05 ppm arises from a Leu^{46} δ-methyl groups while the one at ~−0.25 ppm stems from the bound ligand. (A) Reference spectrum, no ligand. (B–F) Spectra recorded in the presence of increasing concentrations of AMBOC; the [AMBOC]/[kringle 4] molar ratio is indicated on the right. The inset above spectrum B shows the bound AMBOC multiplet slightly resolution enhanced. Kringle concentration ~1 mM, pH* 7.2, 295 K. Impurity signals are indicated (*).

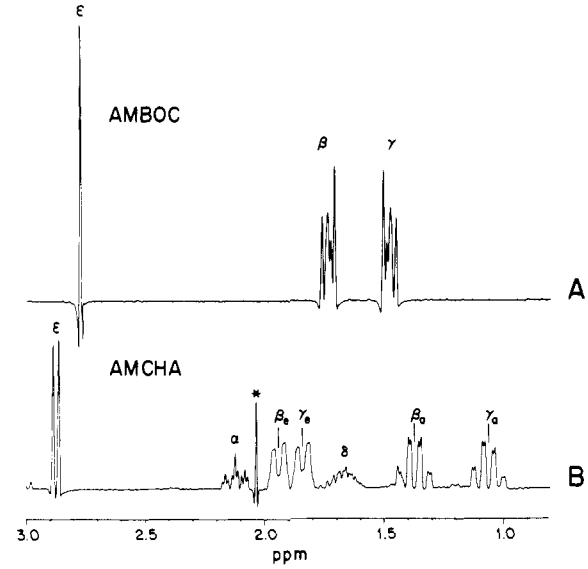

FIGURE 5: ^{1}H NMR spectra of the cyclic ligands AMBOC and AMCHA. Signals are labeled according to their proton origin. For the AMCHA spectrum (B), subscripts a and e denote axial and equatorial, respectively (Jackman & Sternhell, 1969). Spectra were recorded at pH* 7.2, 295 K, and are shown resolution enhanced. An impurity signal is indicated (*).

His^{31}, and His^{33} singlets are shown in Figure 3, which compares the 1D spectrum of ligand-free kringle 4 (B) to those of the kringle saturated with AMBOC (A) and AMCHA (C). Figure 3 also shows the shift of the Trp^{25} H4 doublet which is not included in the COSY expansions shown in Figures 1 and 2. Most interesting is the similar manner in which the His^{33} singlets are perturbed by the two cyclic ligands. The His^{33} H2 resonance moves −0.060 ppm with AMCHA and −0.034 ppm with AMBOC while the H4 resonance moves −0.052 ppm with AMCHA and −0.041 ppm with AMBOC. The lysyl ligands, on the other hand, are much less perturbing (Table I), which suggests an increased steric hindrance against the C$^\beta$ and C$^\gamma$ positions in the case of cyclic ligands. Since Overhauser experiments (vide infra) fail to reveal cross-relaxation between the ligand and His^{33}, the observed effects must reflect secondary effects whereby other side chains are being displaced by the ligand, thus perturbing the imidazole ring. In contrast to what is the case for His^{33}, the His^{31} resonances show only relatively small shifts upon ligand binding (Table I).

Closely related to the effect of ligand binding on the kringle 4 aromatic resonances is the effect of complexation on the ligand itself. Since the binding site is rich in aromatic side chains, one would expect the ligand resonances to experience ring-current shifts upon binding (De Marco et al., 1986, 1987; Ramesh et al., 1987). Figure 4 shows an expansion of the −1.3 ppm $\lesssim \delta \lesssim$ 0.3 ppm spectral region for ligand-free K4 (A) and for K4 in the presence of increasing levels of AMBOC (B–F). Upon minimal additions of ligand, a relatively large resonance appears at ~−0.2 ppm; as the level of ligand is increased, the resonance shifts to lower fields and broadens. Eventually, in the presence of large ligand excess (not shown), the AMBOC spectrum shows up at its free-ligand position (Figure 5A). This behavior is typical of rapid ligand exchange between free and bound states (Sudmeier et al., 1980). In this case the frequency of a ligand resonance at any point of the titration is a weighted average of its frequency in the totally bound state and its frequency in the free state. Therefore, at low concentrations of AMBOC the ligand is mostly bound and the high-field position of the AMBOC resonance reflects the environment of the ligand molecule in the bound state. This shift, of ~1.6 ppm, provides strong evidence for direct ligand–aromatic side chain interactions at the binding site.

The free AMBOC molecule consists of three sets of magnetically equivalent protons and thus yields a relatively simple NMR spectrum (Figure 5A). The six H$^\beta$ and six H$^\gamma$ protons yield well-resolved multiplets at 1.748 and 1.487 ppm, respectively, while the two H$^\delta$ protons yield a singlet at 2.775 ppm. By reference to the molecular structure of AMBOC (Chart II), it is quite possible that in the process of on/off exchange the rigid bicyclic moiety rapidly rotates along its main axis, thus averaging the magnetic environment of the H$^\beta$ and H$^\gamma$ protons. Therefore, the six-proton resonance arising from the bound AMBOC may correspond to the complete set of either H$^\beta$ or H$^\gamma$ protons. Resolution enhancement of the bound AMBOC resonance (Figure 4B, inset) suggests that this resonance is complex. When the spectrum of the free AMBOC is artificially broadened, e.g., via exponential multiplication of the FID (Figure 6B), the H$^\gamma$ multiplet resembles the high-field resonance of the bound AMBOC. The fact that they are not identical (the bound AMBOC H$^\gamma$ protons exhibit a broader spectrum with a slightly different shape) would indicate a contribution of inhomogeneous broadening to its line shape. Overhauser experiments suggest that the resonance from the H$^\beta$ protons of the bound AMBOC overlaps with protein resonances at ~0.45 ppm (Figure 6C).

The experiments discussed above support the highly aromatic character of the binding site indicated by our model (De Marco et al., 1986; Ramesh et al., 1987; Tulinsky et al., 1988). The limited number of aliphatic resonances that are perturbed by ligand binding confirms that most aliphatic residues lie within the peripheral structural framework (Petros et al., 1988a). Therefore, in an attempt to uncover the points of

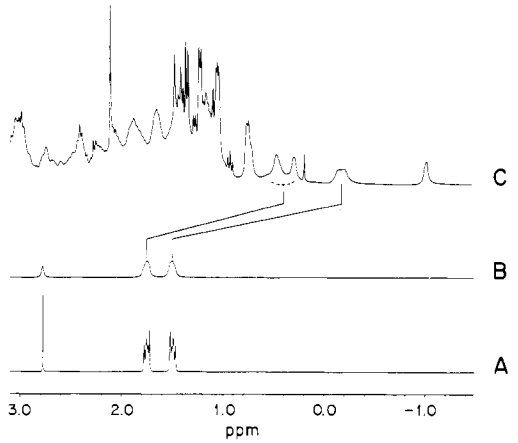

FIGURE 6: ^{1}H NMR spectra of AMBOC: shift and broadening of ligand resonances upon binding to kringle 4. (A) Solution-free AMBOC, no kringle. (B) Spectrum A broadened by exponential multiplication of the FID. (C) AMBOC bound to kringle 4; [ligand]/[kringle] ~0.6, kringle concentration ~1 mM, pH* 7.2, 295 K. Kinked vertical lines connect corresponding resonances in (B) and (C).

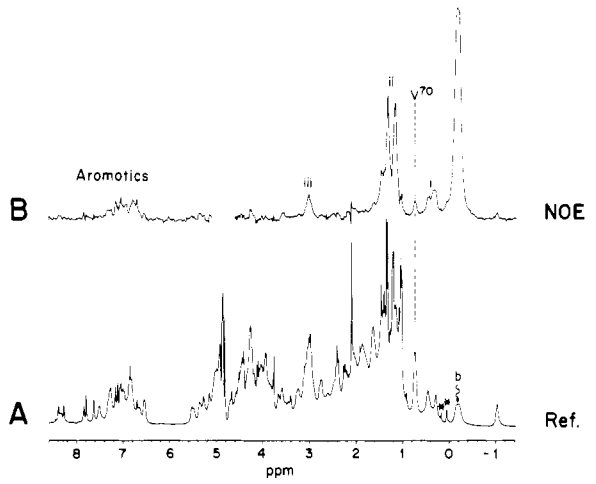

FIGURE 7: ^{1}H NMR spectra of kringle 4 in the presence of AMBOC: ligand–kringle magnetization transfer experiment. (A) Reference spectrum. (B) NOE difference spectrum after 500-ms irradiation of bound AMBOC transition b in spectrum A. Kringle concentration ~5 mM; [ligand]/[kringle] ~0.6, pH* 7.2, 293 K. Impurity signals are indicated (*).

protein–ligand contact, several Overhauser experiments were carried out on K4 complexes with AMBOC and AMCHA.

Ligand–Kringle Saturation Transfer Experiments. Since the shifted AMBOC multiplet is fairly well resolved from kringle signals, it affords a convenient set of transitions to attempt ligand–kringle magnetization transfer (Overhauser) experiments. The high-field multiplet from the bound AMBOC (Figure 4) was irradiated for 500 ms under low-power conditions (see below), and the difference spectrum is presented in Figure 7B. Definite NOEs are apparent in both the aromatic and aliphatic regions of the kringle 4 spectrum. Similar to what is the case with AMBOC, bound AMCHA exhibits a spectrum that is significantly shifted from its free-ligand position (De Marco et al., 1987), extending down to ~−2 ppm (compare Figures 5B and 8B, resonances c–e). Figure 8C–E shows NOE difference spectra after irradiation of the three high-field AMCHA transitions (c–e in spectrum B), for 500 ms, under the same rf power setting as used in the experiment described above for AMBOC. A control experiment (Figure 8A), whereby the rf irradiation was set ~150 Hz to the high-field side of the AMCHA resonances, indicated virtually

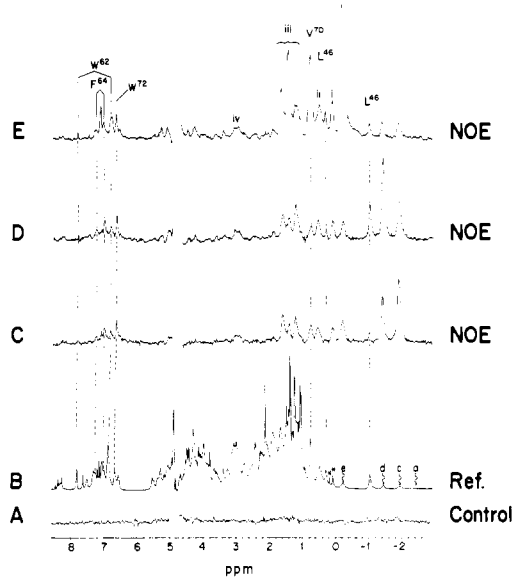

FIGURE 8: ^{1}H NMR spectra of kringle 4 in the presence of AMCHA: ligand–kringle magnetization transfer experiments. (B) Reference: unperturbed kringle spectrum. (C–E) NOE difference spectra after irradiation for 500 ms of transitions stemming from bound AMCHA (resonances c–e in spectrum B). (A) Control NOE spectrum where irradiation was applied at blank position a in spectrum B. Kringle concentration ~5 mM; [ligand]/[kringle] ~0.7, pH* 7.2, 293 K. Impurity signals are indicated (*).

no rf power spillover onto the closest AMCHA transition (resonance c). The three Overhauser difference spectra (C–E) show definite responses in both the aromatic and aliphatic regions. As the irradiation frequency is shifted from ligand peak c to d to e, the experiment is expected to selectively probe different areas of ligand–kringle interaction at the binding pocket. However, despite some minor differences in the pattern of NOE signals obtained upon irradiation of the three transitions, the overall NOE response does not differ significantly for the three experiments, which suggests that only a limited number of side chains contact the ligand. Common to all three experiments are NOEs from Trp^{62}, Phe^{64}, and Trp^{72} (Figure 8E). This is not surprising since, as discussed above, these residues are perturbed strongly by ligand binding (Table I).

A time course study of kringle 4 NOE buildup was carried out for each of the shifted AMCHA resonances. Expansions of the NOE difference spectra obtained for peak d preirradiation (Figure 8B) with rf pulse widths of 100, 250, and 500 ms are shown in Figure 9A–C. The resonances that show the most rapid NOE buildup are those from the Trp^{72} H2, H6, and H7 protons, noticeable even at 100 ms, the shortest irradiation time. Therefore, it is concluded that the Trp^{72} indole ring is in direct contact with the ligand, an interpretation that is consistent with the studies of Hochschwender and Laursen (1981) which showed that chemical modification of this residue interferes with kringle 4 retention by lysine–Sepharose columns. The Phe^{64} H3,5 and Trp^{62} H7 resonances show a moderate NOE buildup rate while the slowest response is for the Trp^{25} H5, Tyr^{74} H2,6, and Trp^{62} H2 resonances. This adds support to our proposed model, wherein Trp^{62}, Phe^{64}, and Trp^{72} are assigned a major role in interacting with the ligand, with Trp^{25} and Tyr^{74} making peripheral contacts with residues at the site (Ramesh et al., 1987; Tulinsky et al., 1988). Similar results were obtained upon irradiation of the other two AMCHA resonances c and e (Figure 8B). Interestingly, an expansion of the aromatic region shows that essentially the same aromatic resonances respond to irradiation of the bound AMBOC as to irradiation of the bound AMCHA (Figure 9C,D).

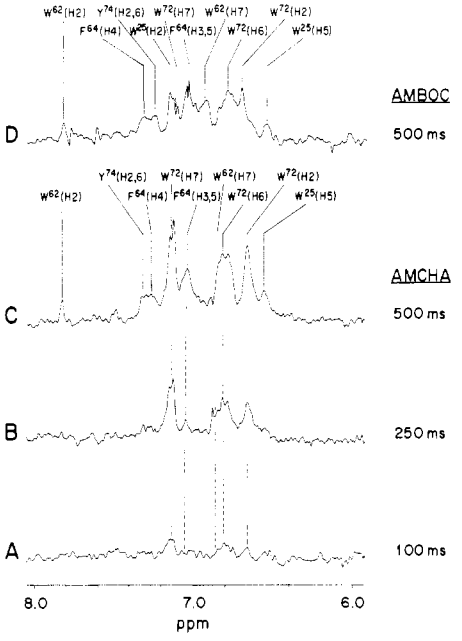

FIGURE 9: ^{1}H NMR spectra of kringle 4 in the presence of AMCHA and AMBOC: ligand–kringle magnetization transfer experiments. (A–C) Buildup of aromatic NOEs upon irradiation of a bound AMCHA transition (resonance e in Figure 8B) for 100 ms (A), 250 ms (B), and 500 ms (C). Dashed lines connect corresponding resonances in the three spectra. (D) Same experiment as (C) except that the irradiated transitions arise from bound AMBOC (multiplet e in Figure 7A). Kringle concentration ~5 mM; [ligand]/[kringle] ~0.7 for AMCHA, ~0.6 for AMBOC, pH* 7.2, 293 K.

Thus, the aromatic side chains that contact AMCHA at the binding site also contact AMBOC. The somewhat decreased kringle NOE intensities of the AMBOC, relative to the AMCHA, complex may well reflect differences in the binding exchange kinetics for the two ligands.

It is also interesting to consider which among the aromatic side chains show negligible NOEs upon irradiation of the bound ligand. The His[33] resonances, which are perturbed by AMCHA binding (Table I), show no detectable NOEs. Therefore, the His[33] ring is unlikely to be in direct contact with the ligand, and its sensitivity to AMCHA probably reflects a conformational displacement of a neighboring side chain. Likewise, the Tyr[41] resonances, which undergo a small high-field shift upon AMCHA binding, do not show up in the NOE difference spectrum. Finally, the Tyr[2], His[3], and Tyr[50] resonances also show no NOEs. As suggested by the prothrombin kringle 1 folding (Park & Tulinsky, 1986), Tyr[2] and His[3] in kringle 4 are likely to be removed from the binding site. However, such is not the case for Tyr[50] since NOESY experiments, as well as molecular modeling, indicate that the Tyr[50] ring is adjacent to Trp[72] (Ramesh et al., 1987). Indeed, we have observed a definite ligand sensitivity of the Tyr[50] spectrum in the case of the plasminogen kringle 5 (Thewes and Llinás, unpublished observations).

Several strong NOEs are observed in the kringle 4 aliphatic spectrum for both the AMBOC and AMCHA experiments (Figures 7 and 8). The response of the Val[70] γ-methyl resonances, which partially overlap at ~0.70 ppm, can be readily identified (Figures 7 and 8E). As discussed above, the Trp[72] indole ring is in close dipolar contact with the ligand. Furthermore, Trexler et al. (1982) have shown via chemical modification experiments that it is most likely the Arg[71] side chain which provides the cationic terminal for ligand binding. Thus, although the Val[70] γ-methyl resonances are not detectably perturbed by ligand presence, their response to ligand irradiation is consistent with Val[70] being positioned in the immediate proximity of Arg[71] at the binding site. The Leu[46] δ,δ'-methyl doublets also show up, to a greater or lesser extent, in the NOE difference spectra of kringle 4 + AMCHA and kringle 4 + AMBOC. This may result from some rf power spillover or, more likely, spin diffusion effects since these signals are considerably weaker with shorter irradiation times: the Leu[46] side chain is known to be centered at the kringle 4 hydrophobic core, adjacent to the binding site (De Marco et al., 1985a; Ramesh et al., 1987). No effort was made to identify the origin of the remaining NOEs in the aliphatic region of the difference spectra, labeled i–iii for kringle 4 + AMBOC (Figure 7B) and i–iv for kringle 4 + AMCHA (Figure 8E). It is likely that resonance i in the kringle 4 + AMBOC spectrum (Figure 7B) arises from a broad resonance of the bound ligand, since its chemical shift does not match that of any kringle resonance. An analogous argument applies to multiplet i in the difference spectrum of kringle 4 + AMCHA (Figure 8C–E) as it also does not correspond to any kringle proton. The remaining NOE signals, which occur in a very crowded spectral region, could arise from either the bound ligand or, quite possibly, from Arg[71] which, as already pointed out, provides the cationic terminal for ligand binding.

Analysis of Ligand-Binding Data. Our analysis of kringle 4 ligand titration experiments follows procedures that have been discussed elsewhere (De Marco et al., 1987). The association constants (K_a) for the various ligands are determined by assuming a simple association/dissociation mechanism that involves a single binding site and fast-exchange averaging of the various resonances (Lerch et al., 1980; Markus et al., 1981; De Marco et al., 1986, 1987). We thus assume that ligand binding to kringle 4 satisfies the equilibrium:

$$K + S \underset{k_{off}}{\overset{k_{on}}{\rightleftharpoons}} KS \qquad (1)$$

where K stands for the unligated kringle, S for the free ligand, KS for the kringle–ligand complex, and $K_a = k_{on}/k_{off}$. If $[K_0]$ denotes the total (=free + bound) kringle concentration, then $\Delta_p \equiv [KS]/[K_0]$, the fraction of ligand-bound kringle, can be derived from the NMR data:

$$\Delta_p = (\delta_{obsd} - \delta_{free})/(\delta_{bound} - \delta_{free}) \qquad (2)$$

where δ_{obsd} is the observed chemical shift of a protein resonance at a certain point of the titration experiment, δ_{free} is the chemical shift of the resonance for the free kringle, and δ_{bound} is the limit chemical shift for the fully complexed kringle. A plot of Δ_p as a function of ligand concentration yields a typical hyperbolic saturation profile. For each ligand we have monitored the response of a number of kringle 4 resonances and calculated an average titration curve. By averaging the ligand response data, it is expected that deviations arising from weak, nonspecific binding and/or from ligand interference with kringle self-aggregation will tend to cancel out. Kringle 4 ligand-binding curves for AMCHA, AMBOC, LysME, and AcLysME are shown in Figure 10.

Substitution of Δ_p into the expression for the Langmuir adsorption isotherm yields (De Marco et al., 1987)

$$\Delta_p^{-1} = 1 + 1/K_a([S_0] - [K_0]\Delta_p)(corr) \qquad (3)$$

where $[S_0]$ stands for the total ligand concentration if the volume were kept constant and (corr) is a factor that corrects for dilution effects. A plot of eq 3, for the ligand AMBOC, is shown in Figure 11; the slope yields a good estimate of K_a^{-1}. The same linear fittings were carried out for LysME, AcLysME, and LysHA. K_a values for these four ligands, along

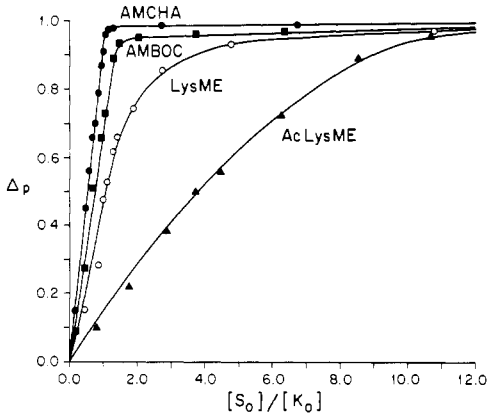

FIGURE 10: Ligand titration profiles of kringle 4. Δ_p, the fraction of kringle with bound ligand, is plotted against $[S_0]/[K_0]$, the ratio of total ligand concentration to total kringle concentration: AMCHA (●), AMBOC (■), LysME (○), and AcLysME (▲). Kringle concentration ~1 mM, pH* 7.2, 295 K.

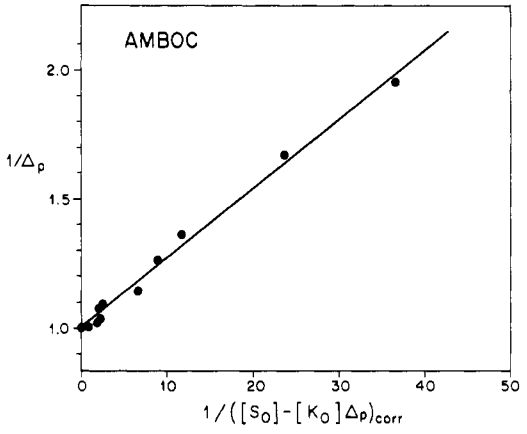

FIGURE 11: Ligand titration of kringle 4 with AMBOC. Straight line results from fitting data to eq 3 (see text), which yields K_a^{-1} from the slope.

Table II: Equilibrium Association and Kinetic Constants for Aliphatic Ligand Binding to Kringle 4 at pH* 7.2, 295 K

ligand	K_a (mM^{-1})[a]	k_{off} (s^{-1})[b]	k_{on} (M^{-1} s^{-1})[c]
L-Lys[d,e]	24.4 ± 2.5		
D-Lys[d,e]	1.2 ± 0.2		
AcLys[d]	37 ± 1	(4.0 ± 0.2) × 10^3	(1.5 ± 0.1) × 10^8
LysME[e]	1.5 ± 0.3		
AcLysME[e]	0.2 ± 0.05		
LysHA[e]	2.0 ± 0.3		
εACA[d]	21 ± 1	(5.3 ± 0.3) × 10^3	(1.1 ● 0.1) × 10^8
AMCHA[d]	159 ± 2	(1.3 ± 0.3) × 10^3	(2.0 ± 0.1) × 10^8
AMBOC	48 ± 2	(3.8 ± 0.3) × 10^3	(1.8 ± 0.1) × 10^8

[a] Determined from linear fittings to eq 3. [b] Determined from linear fittings to eq 4. [c] Calculated from $k_{on} = K_a k_{off}$. [d] Data taken from previous publications (De Marco et al., 1987; Ramesh et al., 1987). [e] Values for k_{off} were not determined; thus, the corresponding k_{on} values are also not listed (see text).

with those for AMCHA, AcLys, D-Lys, L-Lys, and εACA, are listed in Table II.

It is also possible to derive association/dissociation rate constants from the ligand titration data by monitoring the progressive broadening of the bound ligand resonances. As derived by Sudmeier et al. (1980), the excess line broadening ΔW during protein–ligand complexation, is given by

$$\Delta W = (4\pi)\Delta\nu^2 P(1 - P)^2/k_{off} \quad (4)$$

where P ($=\Delta_p[K_0]/[S_0]$) is the fractional population of kringle-bound ligand and $\Delta\nu$ is the ligand chemical shift difference, in hertz, between its free and bound states. Thus, k_{off} values

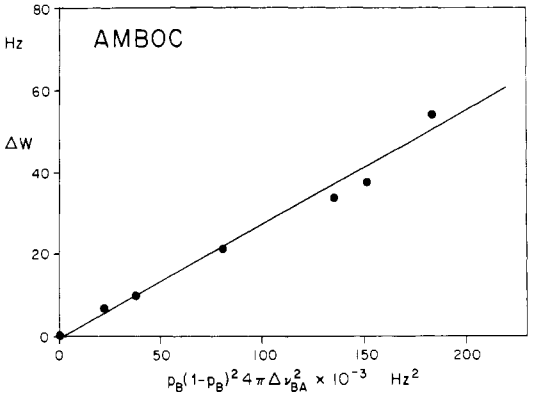

FIGURE 12: Ligand titration of kringle 4 with AMBOC. Straight line results from fitting data to eq 4 (see text), which yields k_{off}^{-1} from the slope.

can be obtained from a linear fitting to eq 4. Figure 12 shows such a plot for AMBOC. The k_{off} and k_{on} ($=K_a k_{off}$) values for AMBOC, AMCHA, and AcLys are listed in Table II.

For the other investigated ligands, LysME, AcLysME, and LysHA, kinetic constants could not be obtained. When LysME binds to kringle 4, four broad resonances appear between about 0 and −1 ppm, in analogy to what is seen for AMCHA, AMBOC, and AcLys. As more ligand is added, these resonances increase in intensity and shift to low field. However, in contrast to what is observed for the latter three ligands, broadening cannot be detected for the resonances from the bound LysME. Presumably, they broaden after they have shifted to overlap with protein signals. For LysHA, a small broad resonance appears at ~−0.5 ppm, about halfway to saturation, but it quickly broadens out, making it unsuitable for accurate measurements of ΔW. Similarly, when kringle 4 is titrated with AcLysME, three high-field resonances appear about midway through the titration, but they broaden and disappear too soon to be of use for a k_{off} determination.

Conclusions

A comparison of association and kinetic constants for the investigated ligands provides insights into both the structure of the kringle 4 binding site and the steric and electrostatic charge requirements of the "optimal" ligand. As the data in Table II indicate, AMCHA is the ligand that interacts most strongly with kringle 4 (K_a ~ 159 mM^{-1}). Indeed, the kringle 4 affinity for AMCHA is ~7.6-fold greater than that for εACA (K_a ~ 21 mM^{-1}). This suggests that hydrophobic contacts probably play an important role in the ligand–kringle 4 interaction since AMCHA has a significantly larger lipophilic surface than εACA. Furthermore, the values for K_a are in line with the idea that the optimal ligand dipole distance is ~6.8 Å (Winn et al., 1980). AMBOC, on the other hand, binds only about one-third as tightly as AMCHA, despite its large hydrocarbon surface and about equal dipole length. The decreased affinity of AMBOC with respect to AMCHA is probably a manifestation of the decreased flexibility of the AMBOC molecule as compared to AMCHA since the latter exhibits chair ⇄ boat isomerism which potentially allows it to better adapt to the topology of the binding site. Indeed, assuming that one of these structures optimally fits the binding site, it would contribute a favorable entropic component to the stability of the interaction, especially vis à vis the flexible linear ligands, which would have to undergo more of a conformational change to dock at the binding pocket.

Inspection of Table II indicates that the higher affinity of kringle 4 for AMCHA relative to AMBOC stems from a more

rapid dissociation of the bicyclic ligand whose k_{off} is $\sim 3.8 \times 10^3$ s^{-1} compared to $\sim 1.3 \times 10^3$ s^{-1} for AMCHA; in both cases the values for k_{on} show that the association is essentially diffusion controlled. Since AMBOC is bulkier than AMCHA, it might be expected to exhibit a more constrained fit at the binding site. The higher value for the AMBOC k_{off} may also explain the relatively weaker NOE irradiation of this ligand elicits on the kringle 4 aromatic resonances when compared with that which results from irradiation of bound AMCHA (Figure 9C,D).

Comparison of the kringle 4 affinities for the various lysyl ligands indicates that AcLys binds the most strongly ($K_a \sim 37$ mM^{-1}), followed by L-Lys ($K_a \sim 24$ mM^{-1}) and ϵACA ($K_a \sim 21$ mM^{-1}), while LysME ($K_a \sim 1.5$ mM^{-1}) and LysHA ($K_a \sim 2.0$ mM^{-1}) interact weakly, and AcLysME ($K_a \sim 0.2$ mM^{-1}) binds the weakest. Thus, the results clearly indicate that the negatively charged carboxyl group is essential for good binding to kringle 4. Consistent with this interpretation is the observation that hexylamine shows essentially no interaction with kringle 4 (M. Rejante and M. Llinás, unpublished observations).

Since the kringle domains appear to mediate the attachment of plasminogen and plasmin to fibrin (Thorsen et al., 1981; Lucas et al., 1983; Väli & Patthy, 1984; Sugiyama et al., 1987), there are three possible lysine-mediated interactions which can be envisioned in vivo. Kringles could bind to (a) an amino-terminal, (b) a carboxy-terminal, or (c) an internal lysyl residue. These different situations are suitably modeled by the ligands (a) LysME, (b) AcLys, and (c) AcLysME, respectively. On the basis of affinity chromatography evidence, Christensen (1984) suggested that fibrinolysis progresses via the interaction of the plasmin(ogen) lysine-binding sites with the carboxy-terminal lysine residues of fibrin which are exposed by plasmin cleavage. Our study provides strong support for this hypothesis since we find that AcLys binds far more tightly to kringle 4 than LysME or AcLysME do. The data for LysHA and the somewhat weaker binding of L-Lys relative to AcLys are also fully consistent with this view.

Registry No. AcLys, 1946-82-3; LysME, 687-64-9; AcLysME, 6072-02-2; LysHA, 25125-92-2; AMCHA, 35015-72-6; AMBOC, 24306-54-5; plasminogen, 9001-91-6.

REFERENCES

Bok, R. A., & Mangel, W. F. (1985) *Biochemistry 24*, 3279–3286.

Brockway, W. J., & Castellino, F. J. (1972) *Arch. Biochem. Biophys. 151*, 194–199.

Castellino, F. J., Ploplis, V. A., Powell, J. R., & Strickland, D. K. (1981) *J. Biol. Chem. 256*, 4778–4782.

Christensen, U. (1984) *Biochem. J. 223*, 413–421.

Claeys, H., Sottrup-Jensen, L., Zajdel, M., Petersen, T. E., & Magnusson, S. (1976) *FEBS Lett. 61*, 20–24.

Collen, D. (1980) *Thromb. Haemostasis 43*, 77–89.

De Marco, A. (1977) *J. Magn. Reson. 26*, 527–528.

De Marco, A., Laursen, R. A., & Llinás, M. (1985a) *Biochim. Biophys. Acta 827*, 369–380.

De Marco, A., Pluck, N. D., Bányai, L., Trexler, M., Laursen, R. A., Patthy, L., Llinás, L., & Williams, R. J. P. (1985b) *Biochemistry 24*, 748–753.

De Marco, A., Laursen, R. A., & Llinás, M. (1986) *Arch. Biochem. Biophys. 244*, 727–741.

De Marco, A., Petros, A. M., Laursen, R. A., & Llinás, M. (1987) *Eur. Biophys. J. 14*, 359–368.

Deutsch, D. G., & Mertz, E. T. (1970) *Science (Washington, D.C.) 170*, 1095–1096.

Dubs, A., Wagner, G., & Wüthrich, K. (1979) *Biochim. Biophys. Acta 577*, 177–194.

Ferrige, A. G., & Lindon, J. C. (1978) *J. Magn. Reson. 31*, 337–340.

Hochschwender, S. M., & Laursen, R. A. (1981) *J. Biol. Chem. 256*, 11172–11176.

Hochschwender, S. M., Laursen, R. A., De Marco, A., & Llinás, M. (1983) *Arch. Biochem. Biophys. 223*, 58–67.

Jackman, L. M., & Sternhell, S. (1969) *Applications of Nuclear Magnetic Resonance Spectroscopy in Organic Chemistry*, pp 238–241, Pergamon Press, Braunschweig.

Lerch, P. G., Rickli, E. E., Lergier, W., & Gillessen, D. (1980) *Eur. J. Biochem. 107*, 7–13.

Llinás, M., Motta, A., De Marco, A., & Laursen, R. A. (1985) *Proc. Int. Symp. Biomol. Struct. Interact., Suppl., J. Biosci. 8*, 121–139.

Lucas, M. A., Fretto, L. J. & McKee, P. D. (1983) *J. Biol. Chem. 258*, 4249–4256.

Markus, G., Camiolo, S. M., Sottrup-Jensen, L., & Magnusson, S. (1981) *Prog. Fibrinolysis 5*, 125–128.

Markwardt, F. (1978) in *Fibrinolytics and Antifibrinolytics* (Markwardt, F., Ed.) pp 511–577, Springer, Berlin.

Motta, A., Laursen, R. A., Llinás, M., Tulinsky, A., & Park, C. H. (1987) *Biochemistry 26*, 3827–3836.

Nagayama, K., Kumar, A., Wüthrich, K., & Ernst, R. (1980) *J. Magn. Reson. 40*, 321–334.

Novokhatny, V. V., Kudinov, S. A., & Privalov, P. L. (1984) *J. Mol. Biol. 179*, 215–232.

Okamoto, S., Oshiba, S., Mihara, H., & Okamoto, U. (1968) *Ann. N.Y. Acad. Sci. 146*, 414–429.

Park, C. H., & Tulinsky, A. (1986) *Biochemistry 25*, 3977–3982.

Petros, A. M., Gyenes, M., Patthy, L., & Llinás, M. (1988a) *Eur. J. Biochem. 170*, 549–563.

Petros, A. M., Gyenes, M., Patthy, L., & Llinás, M. (1988b) *Arch. Biochem. Biophys. 264*, 192–202.

Ramesh, V., Gyenes, M., Patthy, L., & Llinás, M. (1986) *Eur. J. Biochem. 159*, 581–595.

Ramesh, V., Petros, A. M., Llinás, M., Tulinsky, A., & Park, C. H. (1987) *J. Mol. Biol. 198*, 481–498.

Sottrup-Jensen, L., Claeys, H., Zajdel, M., Petersen, T. E., & Magnusson, S. (1978) *Prog. Chem. Fibrinolysis Thrombolysis 3*, 191–209.

Sudmeier, J. L., Evelhoch, J. L., & Jonsson, N. B. H. (1980) *J. Magn. Reson. 40*, 377–390.

Sugiyama, M., Iwamoto, M., & Abiko, Y. (1987) *Thromb. Res. 47*, 459–468.

Thorsen, S., Clemmensen, I., Sottrup-Jensen, L., & Magnusson, S. (1981) *Biochim. Biophys. Acta 668*, 377–387.

Trexler, M., & Patthy, L. (1983) *Proc. Natl. Acad. Sci. U.S.A. 280*, 2457–2461.

Trexler, M., Väli, Z., & Patthy, L. (1982) *J. Biol. Chem. 257*, 7401–7406.

Tulinsky, A., Park, C. H., Mao, B., & Llinás, M. (1988) *Proteins: Struct. Funct., Genet. 3*, 85–96.

Väli, Z., & Patthy, L. (1984) *J. Biol. Chem. 259*, 13690–13694.

Wallén, P. (1980) in *Fibrinolysis* (Kline, D. L., & Reddy, K. N., Eds.) pp 1–24, CRC Press, Boca Raton, FL.

Wider, G., Macura, S., Kumar, A., Ernst, R., & Wüthrich, K. (1984) *J. Magn. Reson. 56*, 207–234.

Wiman, B., & Collen, D. (1978) *Nature (London) 272*, 549–550.

Winn, E. S., Hu, S. P., Hochschwender, S. M., & Laursen, R. A. (1980) *Eur. J. Biochem. 104*, 579–586.